Front. Environ. Sci. Eng. 2020, 14(3): 43
https://doi.org/10.1007/s11783-020-1220-6

RESEARCH ARTICLE

Sorption of aromatic organophosphate flame retardants on thermally and hydrothermally produced biochars

Ziwen Du[1], Chuyi Huang[1], Jiaqi Meng[1], Yaru Yuan[2], Ze Yin[1], Li Feng[1], Yongze Liu[1], Liqiu Zhang (✉)[1]

1 Beijing Key Laboratory for Source Control Technology of Water Pollution, Engineering Research Center for Water Pollution Source Control and Eco-remediation, Beijing Forestry University, Beijing 100083, China
2 College of Environmental Science and Engineering, North China Electric Power University, Beijing 102206, China

HIGHLIGHTS

- TPhP showed faster and higher sorption on biochars than TPPO.
- Pyrochars had higher sorption capacity for TPPO than hydrochar.
- Hydrophobic interactions dominated TPhP sorption by biochars.
- The π-π EDA and electrostatic interactions are involved in sorption.

ARTICLE INFO

Article history:
Received 12 July 2019
Revised 7 November 2019
Accepted 7 January 2020
Available online 6 March 2020

Keywords:
Organophosphate flame retardants
Hydrochar
Pyrochar
Adsorption
Emerging contaminants
Biochar

GRAPHIC ABSTRACT

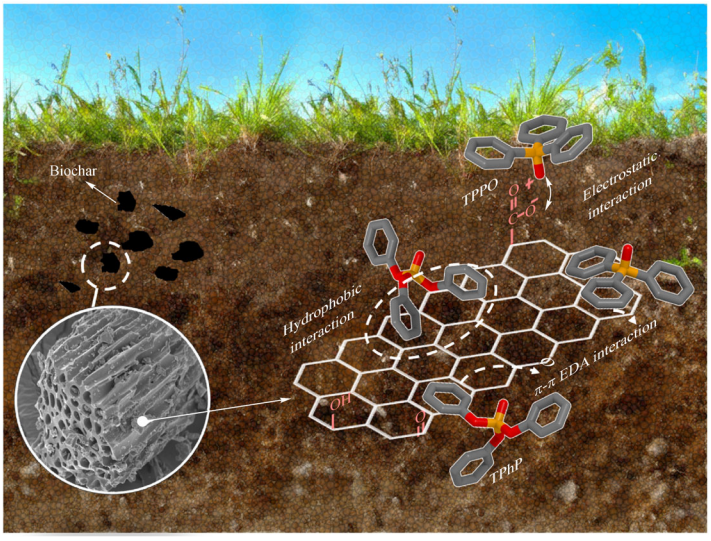

ABSTRACT

Aromatic organophosphate flame retardant (OPFR) pollutants and biochars are commonly present and continually released into soils due to their increasingly wide applications. In this study, for the first time, the sorption of OPFRs on biochars was investigated. Although triphenyl phosphate (TPhP) and triphenylphosphine oxide (TPPO) have similar molecular structures and sizes, TPhP exhibited much faster and higher sorption than TPPO due to its stronger hydrophobicity, suggesting the dominant role of hydrophobic interactions in TPhP sorption. The π-π electron donor–acceptor (EDA) interactions also contributed to the sorption process, as suggested by the negative correlation between the sorption capacity of the aromatic OPFRs and the aromatic index (H/C atomic ratios) of biochar. Density functional theory calculations further showed that one benzene ring of aromatic OPFRs has no electrons, which may interact with biochar via π-π EDA interactions. The electrostatic attraction between the protonated *P* = O in OPFRs and the negatively charged biochar was found to occur at pH below 7. This work provides insights into the sorption behaviors and mechanisms of aromatic OPFRs by biochars.

© Higher Education Press and Springer-Verlag GmbH Germany, part of Springer Nature 2020

1 Introduction

Organophosphate flame retardants (OPFRs) are widely used in various consumer products, such as plastics, textiles, furniture, electronics, and building materials (van der Veen and de Boer, 2012). Due to the ban on polybrominated diphenyl ethers (PBDEs) as flame retardants, the global annual consumption of OPFRs has increased exponentially in recent years (Salamova et al., 2014). The global annual consumption of OPFRs reached 405,000 tons in 2016, and it is expected to grow at a global

✉ Corresponding author
E-mail: zhangliqiu@bjfu.edu.cn

annualized rate of 3.1% (On-Line). OPFRs are physically added to the materials; consequently, they are readily released into the environment over time (Li et al., 2017). OPFRs have been detected globally in various environments, including the atmosphere, water, soil, sediment, fish, as well as human blood, milk, and placenta (van der Veen and de Boer, 2012; Ding et al., 2016; Cao et al., 2017; Greaves and Letcher, 2017; Li et al., 2017). Soil is a major sink for OPFRs (Ji et al., 2019). OPFRs are released into soils through irrigation with wastewater or river water, the disposal of sewage sludge, and wet and dry deposition (Mihajlović et al., 2011; Wei et al., 2015; Ji et al., 2019). The concentration of 12 OPFRs detected in a farmland soil in Northern China was in the range of 0.543–54.9 μg/kg (Ji et al., 2019). Aromatic OPFRs tend to concentrate in the soil more readily than aliphatic OPFRs, because they have low water solubilities and relatively high values of octanol–water partitioning coefficients (Mihajlović et al., 2011); thus, they have high potentials to associate with soil components. Among the aromatic OPFRs detected in farmland soils, triphenyl phosphate (TPhP) contributed the most (Ji et al., 2019).

OPFRs were recognized to have variable bioaccumulation potentials with bioconcentration factors (BCFs) ranging from 0.425 to 1.00 $\times$ 10^6 (Hou et al., 2016). Aromatic OPFRs generally have relatively higher BCFs than chlorinated OPFRs (van der Veen and de Boer, 2012). The accumulation of OPFRs in soil has raised great concerns about their toxic effects on ecosystems and human health via the food chain; in addition, the risks associated with OPFR release is further heightened by their environmental persistence (van der Veen and de Boer, 2012; Wan et al., 2016; Greaves and Letcher, 2017; Fang et al., 2018). Moreover, the fate, toxicity, and bioavailability of organic contaminants in soil are largely controlled by their sorption onto soil components (Jin et al., 2018b; Xiang et al., 2019). Thus, it is of great importance to examine the sorption behavior of OPFRs in soil.

Biochar is a carbon-rich and porous material derived from the carbonization of biomass residues; it is widely present in soil and can comprise up to 45% of soil organic carbon (OC) (Schmidt and Noack, 2000; Jacobson, 2001; Hockaday et al., 2007). In addition, the application of biochar in soils has aroused increasing attention due to its multiple social, financial, and environmental benefits, covering waste biomass management, carbon sequestration, soil improvement, and environmental remediation (Jin et al., 2018a; Lehmann and Joseph, 2015). Biochar has been recognized as a strong sorbent for aromatic organic contaminants, such as polycyclic aromatic hydrocarbons (PAHs), pesticides, and phthalic acid esters (Sun et al., 2012; Jin et al., 2016; Jin et al., 2017), which could be attributed to the high surface hydrophobicity, large surface area, and abundant aromatic components of biochars. Therefore, it appears reasonable to hypothesize that biochar would exhibit a high sorption affinity for aromatic OPFRs. Their interaction with aromatic OPFRs may greatly affect the fate of aromatic OPFRs in soil. However, as far as we know, the interaction of biochars with aromatic OPFRs has not been reported. The systematic investigation of the sorption behavior of aromatic OPFRs by biochars is critical to predicting the fate of aromatic OPFRs, as well as to evaluate the potential of biochar as a low-cost adsorbent to control the migration of aromatic OPFRs in agricultural soils. Recent studies have reported the sorption of OPFRs onto activated carbons and carbon nanotubes (Yan et al., 2014; Wang et al., 2018). The hydrophobicity of OPFRs has been detected to dominate their sorption onto carbon materials (Yan et al., 2014; Wang et al., 2018). The π–π electron donor–acceptor (EDA) interactions were also involved in the interaction between carbon nanotubes and aromatic OPFRs (Yan et al., 2014). The hydrophobic interactions and π–π EDA interactions are also expected to regulate the sorption of aromatic OPFRs by biochars.

In this study, two typical aromatic OPFRs, TPhP, which has a high hydrophobicity, and triphenylphosphine oxide (TPPO), which has a comparatively low hydrophobicity, were selected as model aromatic OPFRs. Two types of biochars: pyrochar and hydrochar, produced from rice straw, were used as sorbents. The specific objectives of this study are (1) to examine the effects of the biochar properties on the sorption behavior of aromatic OPFRs, and (2) to elucidate the role of hydrophobic interactions and π–π EDA interactions in the sorption of aromatic OPFRs by biochars.

2 Material and methods

2.1 Chemicals and materials

TPhP and TPPO (purity>98%) were purchased from Sinopharm Chemical Reagent Co., Ltd. (China). The molecular structures and selected physicochemical properties of the aromatic OPFRs are shown in Table S1. Methanol (HPLC-grade) was obtained from CNW Technologies GmbH (Germany). Other chemicals used in this study were of analytical reagent grade. All the solutions were prepared using deionized (DI) water produced using a Milli-Q water purification system.

Rice straw was selected as a precursor material for biochar production due to its abundance around the world (Kim and Dale, 2004). And the application of its biochar to soil has received great interest for increased crop productivity and soil remediation (Xiao et al., 2014). After being washed and air-dried, the rice straw materials were stored for biochar production. For pyrochars, the rice straws were charred at 300, 450, and 600°C for 1 h in a closed container under oxygen-limited conditions in a muffle furnace. The pyrolytic temperature was raised to the desired values (300, 450, and 600°C) at a ramp rate of 10°C/min. The obtained pyrochars were washed with DI

water until a neutral pH was achieved, after which they were oven-dried at 105°C. Based on the heat treatment temperatures, the pyrochars were denoted as PRS300, PRS450, and PRS600. For hydrothermal carbonization treatments, 10.0 g of rice straws was weighed into a 100 mL Teflonlined stainless steel autoclave. Thereafter, DI water (50 mL) was added to achieve a solid/liquid ratio of 1:5. The reactors were sealed and heated in an oven at 200°C for 8 h. HTC at 200°C has been proposed as an efficient process to produce hydrochar (Sun et al., 2014). The reactors were subsequently allowed to naturally cool to room temperature in the oven. The produced hydrochar (hereinafter referred to as HRS200) and processed water were separated by centrifugation at 3000 r/min for 10 min. The separated HRS200 samples were dried at 105°C, milled to < 0.25 mm, and stored for further characterization and sorption studies.

2.2 Sorbent characterization

The biochars were characterized using an elemental analyzer, an X-ray photoelectron spectrometer, a N_2 adsorption instrument, a FT-IR spectrophotometer, and a scanning electron microscope (SEM). More details are provided in Supplementary Data.

2.3 Sorption experiments

Batch sorption experiments were conducted in 8 or 40 mL Teflonlined screw cap glass vials at 25°C to explore the sorption behavior of aromatic OPFRs on pyrochars and hydrochar. A fixed amount of sorbent from 3 to 40 mg was added into the vials. The sorption kinetic experiments of OPFRs on HRS200 and PRS450 were conducted at an initial concentration of 1 mg/L. To obtain the sorption isotherms of TPhP and TPPO by the biochars, the test solutions of the solutes at various concentrations (0–1.9 mg/L for TPhP and 0–100 mg/L for TPPO) were prepared by spiking the stock solutions into the background solution, which contained 0.01 M $CaCl_2$ to maintain ionic strength and 200 mg/L NaN_3 to avoid any possible biodegradation. The solid-to-solution ratios were selected to achieve 20%–80% uptake of the initially added solute at equilibrium. Next, the glass vials were shaken in the dark for 8 d. The preliminary test showed that the equilibrium times of TPhP and TPPO were less than 7 d for the biochars (Fig. S1). After equilibrium, 5.0 mL of the mixed samples was withdrawn from each vial and filtrated using a 0.45 m polyethersulfone (PES) membrane (the first 3.5 mL of the filtrate was discard). The control experiments showed that the sorption of OPFRS on the PES membrane was insignificant (recovery>99%). The concentrations of TPhP were measured by high-performance liquid chromatography-tandem mass spectrometry (HPLC-MS/MS). The HPLC-MS/MS running parameters are detailed elsewhere (Wang et al., 2018). The filtrate of TPPO was analyzed by HPLC (Shimadzu LC-2030, reversed-phase C18 column, 5 μm, 4.6 mm × 250 mm, Japan) with a diode array detector operated at 222 nm. Isocratic elution was used to determine the TPPO concentration at a flow rate of 1 mL/min with a mobile phase that consisted of 70% methanol and 30% water. All the experiments coupled with blanks were conducted in duplicate, and the averaged value was adopted. The result of the blank controls indicated that the mass losses of TPhP and TPPO during the sorption process were negligible. Therefore, the amounts of sorbed TPhP and TPPO by the pyrochars and hydrochars were calculated by mass difference.

2.4 Data analysis

The pseudo-first-order order, pseudo-second-order, and intra-particle diffusion models were used to simulate the sorption kinetic process. The sorption isotherms of the OPFRs by the biochars were fitted with Langmuir and Freundlich models. More details can be found in Supplementary Data.

The concentration-dependent sorption distribution cefoficient (K_d), as well as the OC-normalized K_d (K_{oc}) values of OPFRs by the biochars, were calculated at three solute concentrations (C_e = 0.01, 0.1, 1S_w, aqueous solubility of solutes) using Eqs. (1) and (2).

$$K_d = q_e/C_e, \tag{1}$$

$$K_{oc} = K_d/f_{oc}. \tag{2}$$

The relationships among the physiochemical properties of the biochars and the sorption coefficients obtained using the above equations were analyzed using Pearson correlation analysis (SPSS 19.0, SPSS Inc.). The fitting was processed with OriginPro 9.1 software (OriginLab, USA).

2.5 Computational method

Density functional theory (DFT) calculations were performed to explore the π electron densities of TPhP and TPPO. Specifically, Gaussian 09 calculation with b3lyp/6-311 + g (d, p) was applied to obtain an optimum molecular conformation with minimum energy (Frisch et al., 2009; Du et al., 2016). Multiwfn 3.6 was applied to evaluate the contribution of atoms to the highest occupied molecular orbital (HOMO) and the lowest unoccupied molecular orbital (LUMO), as well as the calculation of the molecular orbitals for TPhP and TPPO (Lu and Chen, 2012).

3 Results and discussion

3.1 Properties of pyrochars and hydrochar

Under different pyrolysis processing conditions, the hydrochar and pyrochars differed greatly in bulk and

surface elemental composition, ash content, SA, average pore width, and pore volume (Table 1). The bulk OC contents of the rice straw-derived pyrochars were in the range of 50.6%–52.3% (Table 1), and increased with the heat treatment temperature (HTT), which is consistent with previous studies (Sun et al., 2012; Jin et al., 2016). With increasing the HTT, the contents of polar functional groups of the pyrochars decreased, while the hydrophobicity was enhanced, as indicated by the decreased polarity indexes (O/C and (O + N)/C ratios). Compared with the pyrochars, the hydrochar (HRS200) derived from the same rice straw showed comparable bulk OC content, lower O content, and lower (O + N)/C ratio (Table 1), suggesting the higher hydrophobicity of HRS200. The different elemental compositions of the two types of biochars were further demonstrated by their different H/C ratios. H/C ratio has been proved to be feasible for predicting the aromatic skeletal structure of biochars (Xiao et al., 2016). In comparison with the pyrochars, HRS200 showed a slightly higher H/C ratio (Table 1), implying that HRS200 had a lower degree of condensation. This could be attributed to the different processing conditions for HRS200 and pyrochar production. For the pyrochars, the conversion of the rice straw feedstocks was mainly regulated by the dehydration process with HTT increasing from 300°C to 600°C, resulting in a low H/C ratio. In contrast, the hydrothermal carbonization of the rice straw was predominantly governed by the decarboxylation, leading to an additional loss of O (Han et al., 2016).

The surface elemental composition of the biochars determined by XPS analysis differed distinctly from the bulk elemental composition measured by elemental analysis (Table 1). The OC of the biochars was mainly concentrated on the biochar surface, as indicated by the higher surface OC content of the biochars relative to their corresponding bulk counterpart (Table 1). In addition, the surface polarity ((O + N)/C) of HRS200 was substantially higher than those of the pyrochars (Table 1), which was the opposite of the results of bulk polarity and was inconsistent with a recent study (Han et al., 2016). The high surface polarity of HRS200 was likely due to its low carbonization temperature and high ash content (Table 1). It has been shown that the surface polarity varied inversely with HTT and positively with the ash content (Han et al., 2016; Jin et al., 2016). The deconvolution of the C1s scans (Table S2) further demonstrated that the surface O of HRS200 was primarily contributed by C–O and C = O groups.

The FTIR spectra of the biochars are presented in Fig. S2. For pyrochars, the influence of HTT on their surface functional group distribution was observed (Fig. S2). Specifically, when the HTT increased from 300°C to 600°C, all features related to water (3200–3700 cm^{-1}), oxygenated substituents (1700, 1450, and 1311 cm^{-1}), and aliphatic C (2920 and 2853 cm^{-1}) stretch progressively decline, while those of aromatic C = C (1600 cm^{-1}) and C-H (800 cm^{-1}) stretch increase. These results indicate a lessened polarity and an increased aromaticity of the pyrochars, which was in line with the results of bulk elemental analysis (Table 1). In contrast, aliphatic C-H functional groups and oxygenated substituents were dominated in HRS200. This confirms that HRS200 is more hydrophilic than the pyrochars. The structural differences in terms of surface functional groups between the pyrochar and hydrochar would affect their subsequent sorption behavior.

The N_2-accessible SA values of the pyrochars increased with increasing the HTTs as expected (Table 1). Specifically, as the charring temperature increased from 450 to 600°C, it was noted that the SA value of the pyrochars increased dramatically from 9.8 to 243.7 m^2/g (Table 1), which was due to the formation of graphene-like sheets and nanopores, the complete destruction of aliphatic alkyl and ester CO groups, and the exposure of the aromatic core (Keiluweit et al., 2010; Zhang et al., 2011). In addition, the pyrochars and hydrochar differed notably in SA and pore structures (Table 1 and Fig. 1). The SA of HRS200 was lower than those of PRS450 and PRS600, but was almost twice that of PRS300, despite the fact that PRS300 was produced at a higher temperature. The biochar-water partitioning coefficients (K_d values) of neutral organic compounds were found to be positively correlated with the SA of biochars (Qiu et al., 2015; Hale et al., 2016). It is, therefore, expected that HRS200 would exhibit superior sorption strength for aromatic OPFRs compared to that of PRS300. The average pore width of HRS200 reached 18.4 nm, which is remarkably larger than those of the pyrochars (Table 1). The pore size distribution illustrated in Fig. 1 also clearly demonstrated the different pore structures of the two types of biochars. Most of the HRS200 pores were distributed in the range of 5–20 nm, accounting for 70% of the cumulative pore volume up to 50 nm (Fig. 1). In contrast, the pyrochars, particularly PRS600, showed comparatively high pore volumes at the range of 2–4.5 nm (Fig. 1), which would make a great contribution to the aromatic OPFR sorption by the pyrochars. Nanopore-filling has been identified as the dominant mechanism for the sorption of phenanthrene by pyrochars (Jin et al., 2017).

The SEM images (Fig. S3) clearly indicated that there were significant differences in the surface morphologies of the rice straw-derived hydrochar and pyrochars. Under SEM, the pyrochars were relatively smoothed, rigid, and had an inerratic structure. By comparison, HRS200 particles were small in size and occurred as discrete particles, which was in accordance with the amorphous structure of hydrochar demonstrated in a previous study (Han et al., 2016).

3.2 Sorption kinetics of the aromatic organophosphate flame retardants by the biochars

The sorption kinetics of the aromatic OPFRs on the

Table 1 Bulk and surface elemental composition, surface area (SA), average pore width, and pore volume of the rice straw-derived hydrochar and pyrochars

Samples	Bulk elemental composition							Surface elemental composition							Surface enrichment of C [a)]	SA (m^2/g)	Average pore width (nm)	Pore volume (cm^3/g)
	C(%)	O (%)	N (%)	H (%)	O/C	H/C	(O + N)/C	Ash (%)	C (%)	O (%)	N (%)	Si (%)	Ca (%)	(O + N)/C				
HRS200	48.1	5.4	0.8	4.9	0.11	1.21	0.10	40.8	55.0	34.9	1.7	8.5	0.0	0.50	1.14	6.8	18.4	0.031
PRS300	50.6	24.6	1.2	4.4	0.49	1.05	0.38	19.2	67.8	24.0	2.3	4.7	1.2	0.29	1.34	3.7	13.4	0.012
PRS450	51.7	7.7	1.3	3.1	0.15	0.74	0.13	36.2	57.5	26.4	2.6	11.6	1.8	0.38	1.02	9.8	9.3	0.023
PRS600	52.3	5.9	1.3	1.9	0.11	0.40	0.11	38.6	54.3	27.7	2.0	11.9	4.0	0.41	1.08	243.7	2.3	0.141

Note: a) Surface enrichment of C = C (XPS)/C (elemental analysis). Note that HRS200 represents rice straw-derived hydrochar; PRS300, PRS450, and PRS600 represent the rice straw-derived pyrochars produced at 300°C, 450°C, and 600°C, respectively.

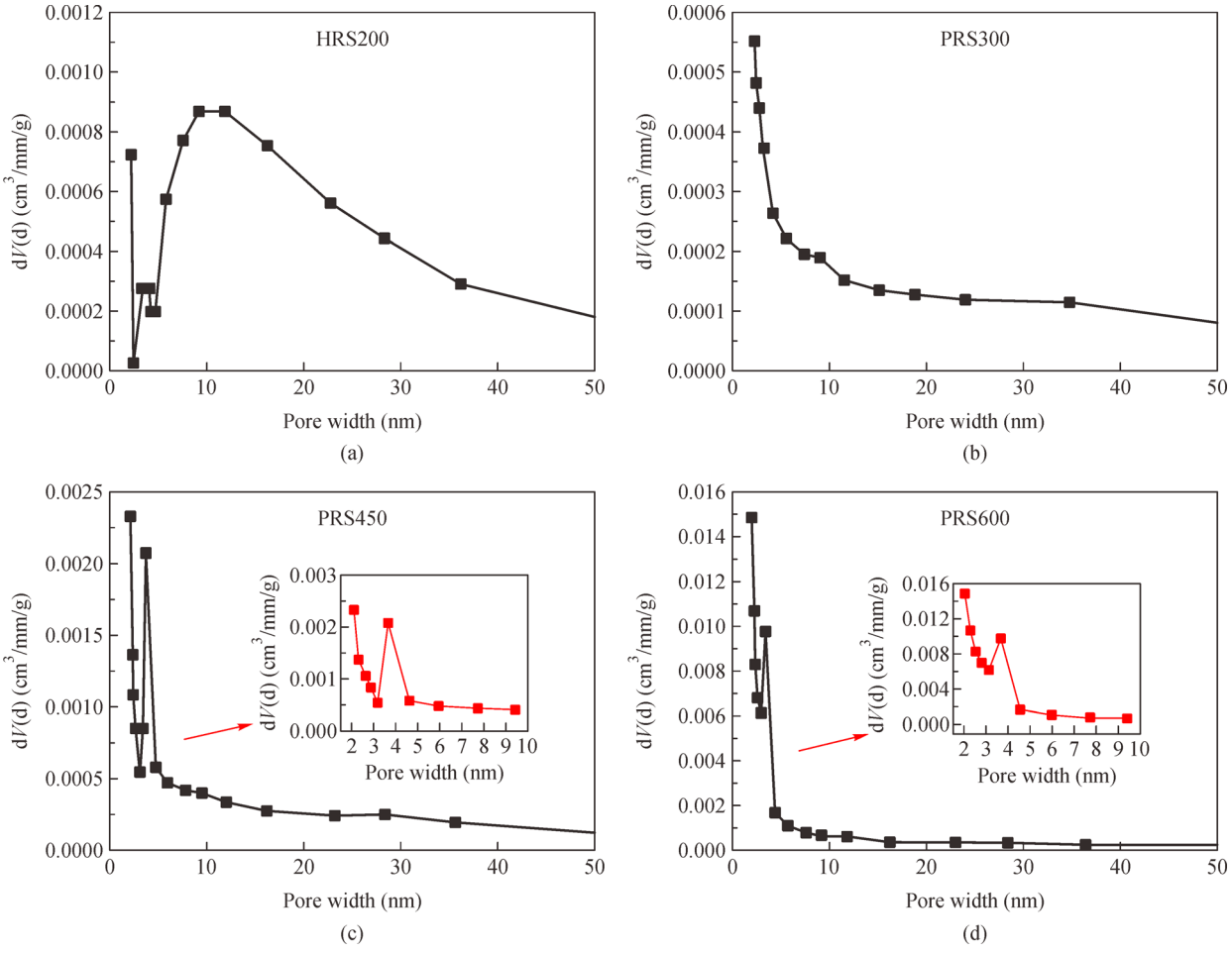

Fig. 1 Pore size distribution of the hydrochar (HRS200) (a) and pyrochars produced at 300 (PRS300) (b), 450 (PRS450) (c), and 600 (PRS600) °C (d).

biochars (Fig. S1) indicate that the sorption equilibrium was achieved within 8 d. To further understand the sorption kinetics, the pseudo-first-order and pseudo-second-order models were applied to fit the sorption kinetic data. The kinetic data were better fitted to the pseudo-second-order model (R^2>0.99) than the pseudo-first-order model (R^2 < 0.73) (Table S3). This implies that the sorption of the aromatic OPFRs on the biochars was likely regulated by chemical interactions, and the sorption capacity was proportional to the amount of active sites on the biochars (Yu et al., 2009). Notably, the initial sorption rates (v_0) of TPhP on the biochars were higher than those of TPPO, indicating that TPhP is more inclined to be sorbed by the biochars, probably due to its high hydrophobicity (logK_{ow} = 4.59). The v_0 values of TPhP on the biochars followed the order of PRS300 < PRS450 < PRS600 (Table S3), which is consistent with the reverse sequence of the bulk polarity and average pore width of the biochars (Table 1). The pyrochar produced at high temperatures had low bulk polarities, shallow pores (Table 1), and thus more active sites, which could facilitate the fast sorption of aromatic OPFRs. Noteworthily, the v_0 value of TPPO on PRS450 was six times larger than that on HRS200 (Table S3), which could be attributed to the smaller pore size of PRS450 (13.4 nm) compared to that of HRS200 (18.4 nm) (Table 1). Small pores can provide more points of contact for organic compounds (Lattao et al., 2014). Additionally, the kinetic data were further fitted to the intra-particle diffusion model to explore the diffusion process of TPPO and TPhP in the biochar systems. As shown in Fig. S4, the slope of q_t versus $t^{1/2}$ yielded two different linear stages. In the first stage, the intra-particle diffusion model satisfactorily fits the kinetic data of TPPO on the biochars with high correlation coefficients and small values of c (the boundary layer thickness coefficient) (Table S3), indicating that intra-particle diffusion may be the rate-limited step in the TPPO sorption by the biochars. In contrast, the intra-particle diffusion model failed to fit the sorption data of TPhP by the biochars according to the poor linearity (R^2 < 0.92) and high c values (Table S3). This implies that besides intra-particle diffusion, other processes, such as the boundary layer diffusion (Wang et al., 2018), may also affect the sorption rate of TPhP on the biochars.

3.3 Effect of solution pH on the sorption of aromatic organophosphate flame retardants

The pH of the aqueous solution will affect the surface charge and the protonation/deprotonation process of the functional groups on the biochars and adsorbates, and consequently the removal of adsorbates. The pH-dependent sorption of TPhP and TPPO by PRS600 was examined over the pH range of 3.0–9.0 (Fig. 2(a)). With increasing the solution pH, the sorption of TPhP and TPPO by PRS600 could be divided into two stages, namely the rapidly increasing stage (stage I) and slow increasing/steady stage (stage II). The amounts of the solutes sorbed on PRS600 increased dramatically with the increase of pH from 3.0 to 7.0 (stage I), and subsequently increase slowly or remained steady at pH>7.0 (stage II) (Fig. 2(a)). The following mechanisms could be used to explain the effect of the solution pH on TPhP and TPPO sorption by PRS600. First, the zeta potential of PRS600 was negative at the studied pH range and became more negative as the pH (Fig. 2(b)) of the aqueous solution increased. This result suggests that on the biochar surface, most O-containing function groups were dissociated. The dissociated species such as $–COO^-$ and $-O^-$ could act as strong *n*-donors in the *n*-EDA interactions with solutes, facilitating their sorption. In addition, the doubly bonded O atom of TPhP and TPPO has a strong affinity for protons in water owing to the high electron cloud density of the O atom, leading to the protonation of the solutes via O-protonation (Vank et al., 2000). At a pH below 7, the negatively charged functional groups on the biochar surface could electrostatically attract the positively charged *P* = O in TPhP and TPPO, thereby enhancing their sorption capacity on the biochar surface. Furthermore, with the rise in the solution pH, there was a noticeable reduction in the aggregation of PRS600 particles (Fig. 2(c)). This was caused by the increased ionization of the biochar surface functional moieties, and thus the higher electrostatic repulsion among biochar particles. As a result, more active sorption sites on PRS600, which was originally shielded due to the strong aggregation of PRS600 particles at lower pH, would be opened up for solute molecules, leading to the sharp rise in sorption with the increase of pH in stage I. In contrast, at a pH above 7, the protonation of O atom in phosphate group was weakened due to the low proton concentration in solution. Meanwhile, the zeta potential of PRS600 only slightly decreased at high a pH (Fig. 2(b)). Consequently, the interactions between the biochar and the solutes at pH values above 7 were only marginally enhanced in stage II.

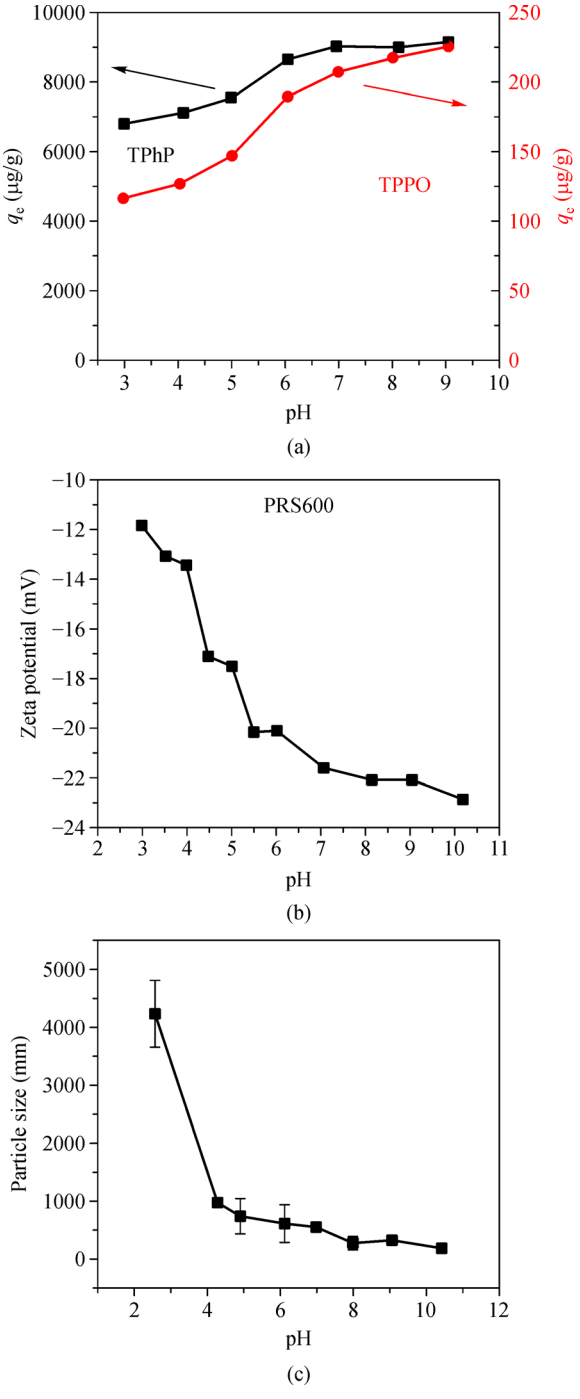

Fig. 2 Effects of the solution pH on the sorption of triphenyl phosphate (TPhP) and triphenylphosphine oxide (TPPO) by the pyrochar produced at 600°C (PRS600) (a); the zeta potentials (b) and particle sizes (c) of PRS600 at different pH values.

3.4 Effect of organophosphate flame retardant properties on sorption

The sorption data of the aromatic OPFRs by the biochars were fitted by Langmuir and Freundlich models (Fig. S5). As summarized in Tables 2 and S4 the sorption behaviors of TPhP and TPPO by the hydrochar and pyrochars can be satisfactorily described by the Freundlich models with high correlation coefficients (R^2) in the range of 0.990–0.998 compared to the case with the Langmuir model (R^2 = 0.969–0.991). The Langmuir model is based on the

assumption that all the sorption sites presented on the sorbent surfaces have equal sorption affinity for solutes. Apparently, it is unsuitable for biochars with many high-energy sorption sites, such as defects, edges, functional groups, and micropores (Abdul et al., 2017).

Based on the Freundlich model, the nonlinearity coefficient (n) values of TPhP and TPPO by the biochars were in the ranges of 0.47–0.52 and 0.44–0.65, respectively (Table 2), suggesting that the sorption of the aromatic OPFRs by the biochars was highly nonlinear. The K_d and K_{oc} values of TPhP by the tested biochars were remarkably higher than those of TPPO (Table 2), which agrees well with their different hydrophobicity (as measured by logK_{ow}, 4.59 vs. 2.87, Table S1) values. This implies that the hydrophobic interactions, which originated from van der Waals forces, regulated the sorption of the aromatic OPFRs by the biochars. To screen out the hydrophobic mechanisms, the K_{oc} values of the solutes were normalized by their corresponding K_{ow} values. After K_{ow} normalization, TPhP still demonstrated higher K_{oc}/K_{ow} values than TPPO for any given biochar (Table 2), indicative of the contribution of other specific sorbate–sorbent interactions, such as H-bonding interactions and π-π EDA interactions.

3.5 Effect of biochar properties on sorption

For a given solute, differences in the sorption behavior also existed among the biochars. For both solutes, a high HTT increased the nonlinearity of the sorption isotherms by the pyrochars (Table 2). For TPPO, the n value of HRS200 was larger than those of the pyrochars (Table 2). The variability in the n values of the biochars could be linked to their different levels of aromaticity, as indicated by the positive relationship between the n value and the aromatic index (H/C atomic ratio) of the biochars (Fig. S6). The H/C atomic ratio has been proposed as a smart linkage between pyrolytic temperatures, aromatic cluster structures, and sorption properties of the biochars derived from diverse precursory materials (Xiao et al., 2016). The adsorption of solutes by the nanovoids within the condensed aromatic domains of biochars is expected to result in nonlinear sorption (Jin et al., 2017; Jin et al., 2018a).

The sorption capacity (K_d and K_{oc} at C_e = 0.01 C_s) of TPPO by HRS200 was lower than those by the pyrochars (Table 2). The result that the hydrochar demonstrated limited sorption capacity in comparison with that of the pyrochar was contrary to the findings of a recent study, that the hydrochars produced at 250°C displayed higher sorption to both nonpolar and polar compounds than the pyrochars obtained at 250°C, 450°C, and 600°C (Han et al., 2016). The inconsistency may be attributed to the different hydrothermal temperatures (200°C vs. 250°C) used for the hydrochar production in the present and previous studies. It is reported that the bamboo hydrochar prepared at 240°C provided noticeably higher sorption for 2-naphthol than that prepared at 200°C (Li et al., 2016). Therefore, the low hydrothermal temperature applied in this study may lead to the limited sorption capacity of the hydrochar. In addition, the high hydrophilicity of HRS200 as indicated by the FT-IR spectra (Fig. S2) was unfavorable for its sorption of HOCs. For the pyrochars, their sorption capacities (K_d and K_{oc} at C_e = 0.01 C_s) for TPhP and TPPO followed the order PRS300 < PRS450 < PRS600 (Table 2). Evidently, the pyrochar produced at a high temperature was more effective in the sorption of the aromatic OPFRs. This agrees with the results from previous studies, that the sorption capacity of aromatic contaminants such as polycyclic aromatic hydrocarbons and herbicides, by pyrochars, increased with increasing HTT (Sun et al., 2013; Xiao et al., 2016). The hidden linkage between the HTT and the biochar sorption behaviors is the biochar structure. With increasing the HTT, the reduction of the bulk polar functional groups, development of micropores, and formation of condensed aromatic clusters were demonstrated in the present and

Table 2 Freundlich isotherm parameters and concentration-dependent distribution coefficients (logK_d and logK_{oc}) for triphenyl phosphate (TPhP) and triphenylphosphine oxide (TPPO) on the hydrochar and pyrochars

Samples	K_F	n	R^2	logK_d (mL/g)			logK_{oc}[a] (mL/g)		K_{oc}/K_{ow}	
				C_e = 0.01 S_w	C_e = 0.1 S_w	C_e = 1 S_w	C_e = 0.01 S_w	C_e = 0.1 S_w	C_e = 1 S_w	C_e = 0.01 S_w
TPhP										
PRS300	268.2±35.5[b]	0.52±0.02	0.992	4.82	4.34	3.86	5.11	4.63	4.16	3.33
PRS450	355.2±0.5	0.50±0.01	0.998	4.92	4.43	3.94	5.21	4.72	4.23	4.17
PRS600	524.7±0.5	0.47±0.02	0.990	5.04	4.51	3.98	5.32	4.79	4.26	5.41
TPPO										
HRS200	2.7±0.6	0.65±0.04	0.991	1.92	1.56	1.21	2.23	1.88	1.53	0.23
PRS300	5.2±2.3	0.61±0.04	0.996	2.04	1.65	1.26	2.33	1.95	1.56	0.29
PRS450	27.0±10.9	0.51±0.04	0.991	2.30	1.81	1.32	2.59	2.10	1.60	0.52
PRS600	60.4±12.5	0.44±0.02	0.994	2.38	1.82	1.27	2.66	2.10	1.55	0.62

Note: a) K_{oc} is the organic carbon (OC)-normalized sorption distributed coefficient (K_d); b) Standard deviation. Note that HRS200 represents rice straw-derived hydrochar; PRS300, PRS450, and PRS600 represent the rice straw-derived pyrochars produced at 300°C, 450°C, and 600°C, respectively.

previous studies (Keiluweit et al., 2010; Xiao et al., 2016). These factors, which can be involved in the biochar-aromatic contaminant interactions via specific adsorption including H-bonding, pore-filling, and π-π EDA interactions, are vital to the sorption behavior of biochars (Hale et al., 2016).

In this study, as expected, significantly negative relationships ($r = -1.00$, $p < 0.001$ for TPhP and $r = -0.97$, $p < 0.05$ for TPPO) were found between the logK_{oc} values ($C_e = 0.01\ S_w$) of the tested aromatic OPFRs and the H/C atomic ratios of all the biochars (Figs. 3(a) and 3(b)). The results suggest that the π-π interactions between the aromatic substituents of the aromatic OPFRs and the aromatic sheet of biochars may contribute substantially to the aromatic OPFR sorption by the biochars. Previous studies (Yan et al., 2014; Wang et al., 2018) found that the sorption amounts of aromatic OPFRs on activated carbons and carbon nanotubes were appreciably higher than those of aliphatic OPFRs, which also suggested the strong π-π EDA interactions between the aromatic OPFRs and the aromatic domains of the carbon materials. Moreover, the results of the electron distribution of TPhP and TPPO, simulated using DFT calculations (Fig. 4(a)), implied the involvement of π-π EDA interactions. The modeling results clearly show that the electrons of TPhP and TPPO are concentrated on two benzene rings, while the third benzene ring has no electrons. The electron-deficient benzene ring may act as a π-acceptor in the interaction with biochars, the aromatic sheets of which have be proved to be able to act as π-donors (Sun et al., 2012). Additionally, the HOMO/LUMO levels are –6.784 eV/–0.672 eV for TPhP and –6.749 eV/–0.864 eV for TPPO, respectively (Fig. 4(a)), verifying that TPhP and TPPO are electron deficient. Therefore, the π-π EDA interactions between the π electron-deficient aromatic OPFRs and the π electron-rich biochars are expected. Additionally, TPhP and TPPO have similar HOMO/LUMO levels, indicating that they had comparable ability to attract electrons. Therefore, the strength of the π-π EDA interactions between the two sorbates and the biochars would also be comparable. Furthermore, the logK_{oc} values ($C_e = 0.01\ S_w$) of the aromatic OPFRs increased with the surface O contents of the pyrochars (Figs. 3(c) and 3(d)). The surface O of the pyrochars may be beneficial for improving the sorption of aromatic OPFRs through n-π EDA interactions and electrostatic interactions as mentioned above. Furthermore, the O-containing functional groups in biochars may act as H-bonding acceptor sites and link to the O atom of the organic compounds through bridging water molecules (Sun et al., 2012). In this study, H-bonding may also contribute to the sorption of the tested solutes on the biochars, but not significantly, particularly for PRS600. PRS600 had the most hydrophobic surface among all the tested biochars; hence, its combination with water molecules by H-bonding was unfavorable.

The sorption of organic compounds to biochars was also declared to have proceeded via a pore-filling mechanism (Nguyen et al., 2007; Jin et al., 2017). Here, for the pyrochars, it could be found that the larger the SA of the pyrochar, the higher the logK_{oc} value ($C_e = 0.01\ S_w$) (Tables 1 and 2). The result highlighted that the SA of the pyrochars may regulate their sorption of TPhP and TPPO. Notably, the hydrochar (HRS200) had lower logK_{oc} values compared with that of PRS300 (Table 2), although the SA of HRS200 (6.8 m^2/g, Table 1) was almost twice that of PRS300 (3.7 m^2/g, Table 1), suggesting that SA alone could not predict the sorption of TPPO by various biochars. In addition to SA, the pore size distribution also affects the pore filling process of organic compounds in rigid porous materials. The maximum diameters of TPPO and TPhP with minimum energy (calculated using Gaussian 09 software) were 0.98 and 1.14 nm, respectively. The biochars with relatively high pore volumes at the range of 2–4.5 nm (Fig. 1) exhibit high sorption for TPPO and TPhP (Table 2), indicating that the nano-pore filling may play a role. Moreover, the filling of small pores involves more points of contact (Lattao et al., 2014). Consequently, organic compounds are more easily entrapped in the small pores within the porous materials. Consistently, it is noted that the logK_{oc} values ($C_e = 0.01\ S_w$) of both hydrochar and pyrochars were negatively correlated with their average pore width (Figs. 3e and 3f), confirming the major contribution of the small pores to the sorption of aromatic OPFRs. The pores of HRS200 were dominated by mesopores with an average pore width of 18.4 nm, which is larger than that of PRS300, which could account for the relatively low sorption capacity of HRS200 (Tables 1 and 2). Furthermore, given that TPPO and TPhP have similar molecular structures and sizes (Table S1), the role of molecular conformation of the solutes on their sorption variation would be insignificant.

According to the above results and discussion about the sorption behaviors, the possible interactions between aromatic OPFRs and biochars were proposed (Fig. 4(b)). Hydrophobic interactions should be dominant in the sorption of aromatic OPFRs by biochars. The electron-deficient benzene ring of aromatic OPFRs may interact with the aromatic sheets of biochar via π-π EDA interactions. Noteworthily, the strength of the π-π EDA interactions between the two aromatic OPFRs and the biochars would be comparable, given that they have similar HOMO/LUMO levels, and thus similar abilities to attract electrons. In addition, the electrostatic interactions may occur between the negatively charged functional groups of the biochars and the positively-charged $P = O$ in aromatic OPFRs at a pH below 7. Moreover, the pore-filling mechanism was probably involved in the sorption process. The contributions of electrostatic interactions and pore-filling mechanism to the TPhP sorption would be comparable to those to the TPPO sorption, considering that

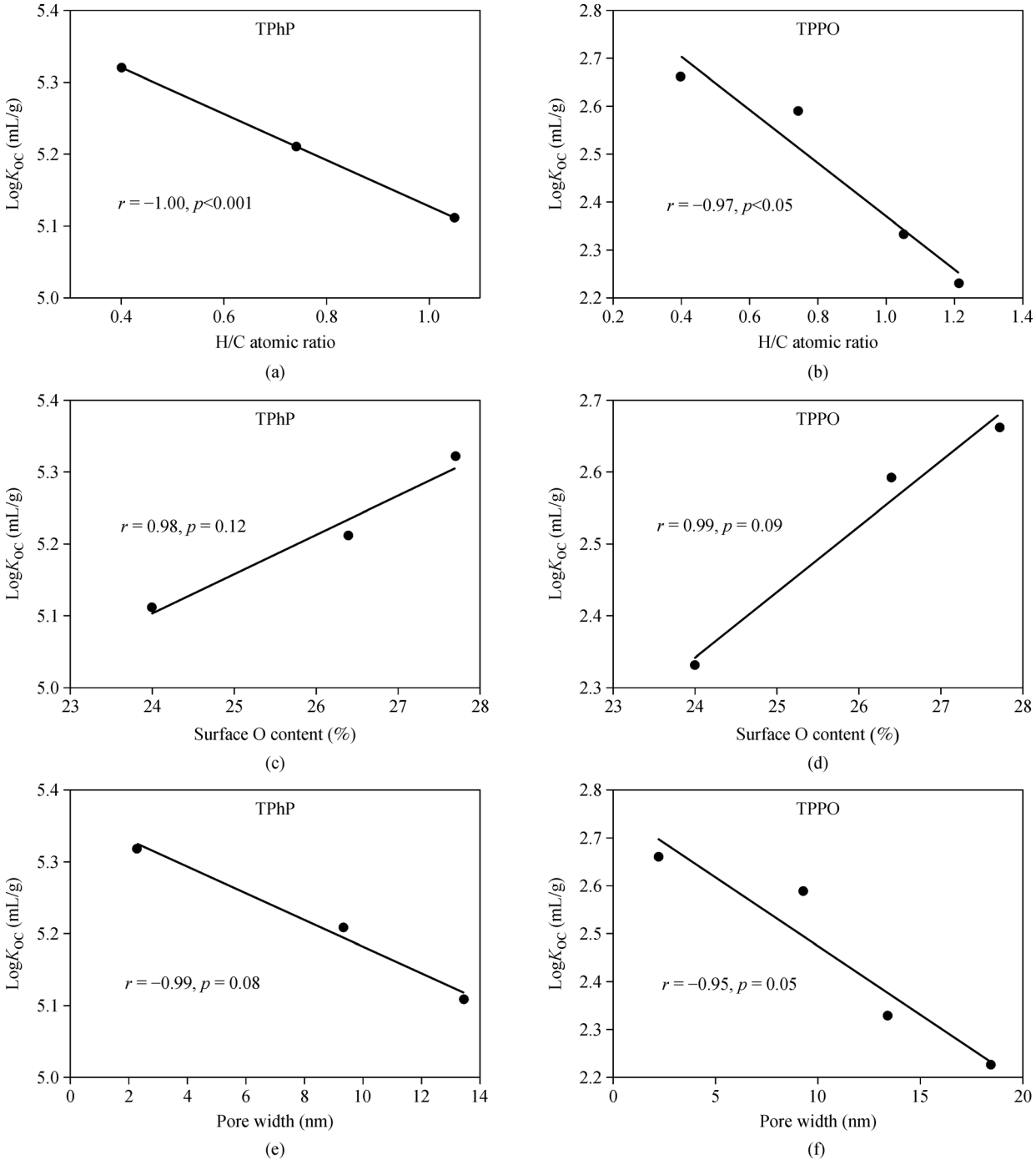

Fig. 3 Correlations between the logK_{oc} values of triphenyl phosphate (TPhP) and triphenylphosphine oxide (TPPO) by the biochars and their H/C atomic ratios (a and b), surface O content measured using XPS (c and d), and average pore width (e and f).

TPhP and TPPO had similar molecular structures and sizes. Therefore, the remarkably higher sorption ability of TPhP, compared to that of TPPO mentioned above, could be mainly attributed to the stronger hydrophobicity of TPhP. In conclusion, for the highly hydrophobic TPhP, hydrophobic interactions should regulate its sorption by biochars. In contrast, TPPO is weakly hydrophobic; various interactions including hydrophobic interactions, π-π EDA interactions, electrostatic attractions, and the pore-filling mechanism may be involved in the TPPO sorption by biochars.

4 Conclusions

This study investigated the sorption of aromatic OPFRs by

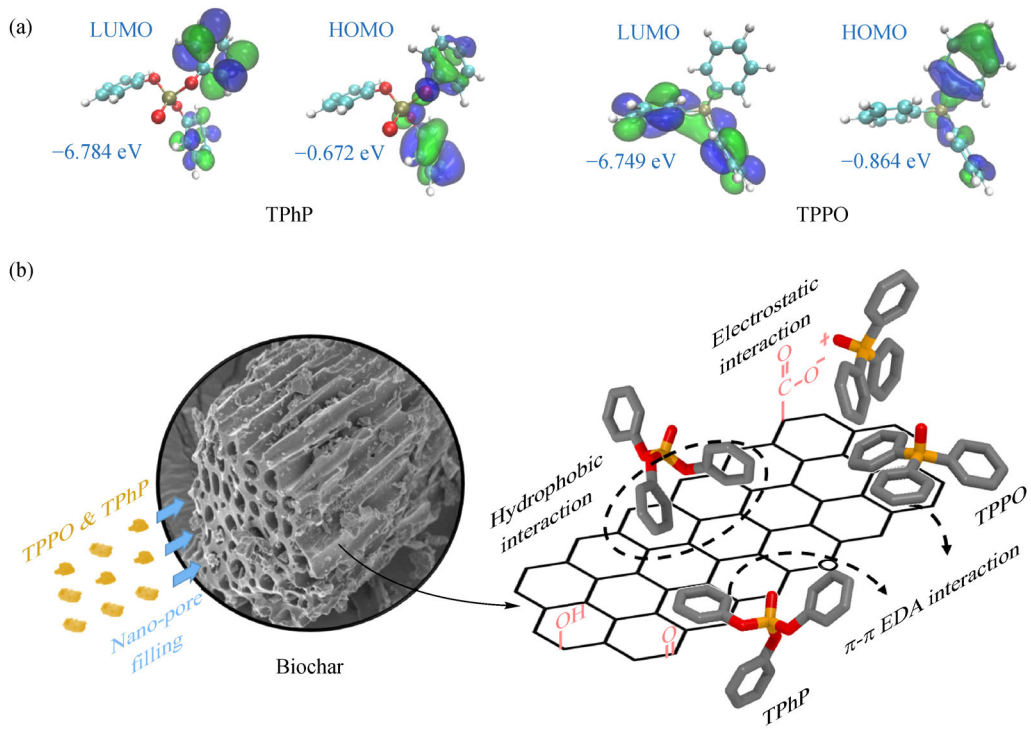

Fig. 4 Highest occupied molecular orbital (HOMO) and lowest unoccupied molecular orbital (LUMO) of triphenyl phosphate (TPhP) and triphenylphosphine oxide (TPPO) (a); sorption mechanisms of TPhP and TPPO onto biochar (b).

biochars. The pyrochars produced at high temperatures exhibited faster and higher sorption than those produced at low temperatures and hydrochar. The π-π EDA interactions occurred between the electron-deficient benzene ring of OPFRs and the aromatic sheets of the biochar. The sorption of aromatic OPFRs increased with increasing solution pH, due to the electrostatic attraction between the protonated *P* = O in OPFRs and the negatively charged biochar surface. The pore-filling mechanism was also probably involved in the sorption process. These findings are helpful for understanding the environmental behavior of aromatic OPFRs in soils and the selection of effective adsorbents for the control of OPFR pollutants.

Acknowledgements This research was supported by the Beijing Natural Science Foundation (No. 8182037), National Natural Science Foundation of China (Grant Nos. 41703097 and 41977317), Fundamental Research Funds for the Central Universities (No. 2018ZY16), and National College Students' innovation and entrepreneurship training program (No. 201810022077).

Electronic Supplementary Material Supplementary material is available in the online version of this article at https://doi.org/10.1007/s11783-020-1220-6 and is accessible for authorized users.

References

Abdul G, Zhu X, Chen B (2017). Structural characteristics of biochar-graphene nanosheet composites and their adsorption performance for phthalic acid esters. Chemical Engineering Journal, 319: 9–20

Cao D, Guo J, Wang Y, Li Z, Liang K, Corcoran M B, Hosseini S, Bonina S M C, Rockne K J, Sturchio N C, Giesy J P, Liu J, Li A, Jiang G (2017). Organophosphate esters in sediment of the Great Lakes. Environmental Science & Technology, 51(3): 1441–1449

Ding J, Xu Z, Huang W, Feng L, Yang F (2016). Organophosphate ester flame retardants and plasticizers in human placenta in Eastern China. Science of the Total Environment, 554–555: 211–217

Du Z, Deng S, Zhang S, Wang B, Huang J, Wang Y, Yu G, Xing B (2016). Selective and high sorption of perfluorooctanesulfonate and perfluorooctanoate by fluorinated alkyl chain modified montmorillonite. Journal of Physical Chemistry C, 120(30): 16782–16790

Fang Y, Kim E, Strathmann T J (2018). Mineral- and base-catalyzed hydrolysis of organophosphate flame retardants: Potential major fate-controlling sink in soil and aquatic environments. Environmental Science & Technology, 52(4): 1997–2006

Frisch M, Trucks G, Schlegel H, Scuseria G, Robb M, Cheeseman J, Scalmani G, Barone V, Mennucci B, Petersson G (2009). GAUSSIAN09. Gaussian Inc., Wallingford, CT, USA

Greaves A K, Letcher R J (2017). A review of organophosphate esters in the environment from biological effects to distribution and fate. Bulletin of Environmental Contamination and Toxicology, 98(1): 2–7

Hale S E, Arp H P H, Kupryianchyk D, Cornelissen G (2016). A synthesis of parameters related to the binding of neutral organic compounds to charcoal. Chemosphere, 144: 65–74

Han L, Ro K S, Sun K, Sun H, Wang Z, Libra J A, Xing B (2016). New evidence for high sorption capacity of hydrochar for hydrophobic organic pollutants. Environmental Science & Technology, 50(24):

13274–13282

Hockaday W C, Grannas A M, Kim S, Hatcher P G (2007). The transformation and mobility of charcoal in a fire-impacted watershed. Geochimica et Cosmochimica Acta, 71(14): 3432–3445

Hou R, Xu Y, Wang Z (2016). Review of OPFRs in animals and humans: Absorption, bioaccumulation, metabolism, and internal exposure research. Chemosphere, 153: 78–90

Jacobson M Z (2001). Strong radiative heating due to the mixing state of black carbon in atmospheric aerosols. Nature, 409(6821): 695–697

Ji Y, Wang Y, Yao Y, Ren C, Lan Z, Fang X, Zhang K, Sun W, Alder A C, Sun H (2019). Occurrence of organophosphate flame retardants in farmland soils from Northern China: Primary source analysis and risk assessment. Environmental Pollution, 247: 832–838

Jin J, Kang M, Sun K, Pan Z, Wu F, Xing B (2016). Properties of biochar-amended soils and their sorption of imidacloprid, isoproturon, and atrazine. Science of the Total Environment, 550: 504–513

Jin J, Li S, Peng X, Liu W, Zhang C, Yang Y, Han L, Du Z, Sun K, Wang X (2018a). HNO_3 modified biochars for uranium (VI) removal from aqueous solution. Bioresource Technology, 256: 247–253

Jin J, Sun K, Wang Z, Han L, Du P, Wang X, Xing B (2017). Effects of chemical oxidation on phenanthrene sorption by grass-and manure-derived biochars. Science of the Total Environment, 598: 789–796

Jin J, Sun K, Yang Y, Wang Z, Han L, Wang X, Wu F, Xing B (2018b). Comparison between soil- and biochar-derived humic acids: Composition, conformation, and phenanthrene sorption. Environmental Science & Technology, 52(4): 1880–1888

Keiluweit M, Nico P S, Johnson M G, Kleber M (2010). Dynamic molecular structure of plant biomass-derived black carbon (biochar). Environmental Science & Technology, 44(4): 1247–1253

Kim S, Dale B E (2004). Global potential bioethanol production from wasted crops and crop residues. Biomass and Bioenergy, 26(4): 361–375

Lattao C, Cao X, Mao J, Schmidt-Rohr K, Pignatello J J (2014). Influence of molecular structure and adsorbent properties on sorption of organic compounds to a temperature series of wood chars. Environmental Science & Technology, 48(9): 4790–4798

Lehmann J, Joseph S (2015). Biochar for Environmental Management: Science, Technology and Implementation. Earthscan: London/New York

Li J, Xie Z, Mi W, Lai S, Tian C, Emeis K C, Ebinghaus R (2017). Organophosphate esters in air, snow, and seawater in the North Atlantic and the Arctic. Environmental Science & Technology, 51 (12): 6887–6896

Li Y, Meas A, Shan S, Yang R, Gai X (2016). Production and optimization of bamboo hydrochars for adsorption of Congo red and 2-naphthol. Bioresource Technology, 207: 379–386

Lu T, Chen F (2012). Multiwfn: A multifunctional wavefunction analyzer. Journal of Computational Chemistry, 33(5): 580–592

Mihajlović I, Miloradov M V, Fries E (2011). Application of Twisselmann extraction, SPME, and GC-MS to assess input sources for organophosphate esters into soil. Environmental Science & Technology, 45(6): 2264–2269

Nguyen T H, Cho H H, Poster D L, Ball W P (2007). Evidence for a pore-filling mechanism in the adsorption of aromatic hydrocarbons to a natural wood char. Environmental Science & Technology, 41(4): 1212–1217

Qiu M, Sun K, Jin J, Gao B, Yan Y, Han L, Wu F, Xing B (2015). Properties of the plant- and manure-derived biochars and their sorption of dibutyl phthalate and phenanthrene. Scientific Reports, 4 (1): 5295

Salamova A, Ma Y, Venier M, Hites R A (2014). High levels of organophosphate flame retardants in the great lakes atmosphere. Environmental Science & Technology Letters, 1(1): 8–14

Schmidt M W, Noack A G (2000). Black carbon in soils and sediments: Analysis, distribution, implications, and current challenges. Global Biogeochemical Cycles, 14(3): 777–793

Sun K, Jin J, Keiluweit M, Kleber M, Wang Z, Pan Z, Xing B (2012). Polar and aliphatic domains regulate sorption of phthalic acid esters (PAEs) to biochars. Bioresource Technology, 118: 120–127

Sun K, Kang M, Zhang Z, Jin J, Wang Z, Pan Z, Xu D, Wu F, Xing B (2013). Impact of deashing treatment on biochar structural properties and potential sorption mechanisms of phenanthrene. Environmental Science & Technology, 47(20): 11473–11481

Sun Y, Gao B, Yao Y, Fang J, Zhang M, Zhou Y, Chen H, Yang L (2014). Effects of feedstock type, production method, and pyrolysis temperature on biochar and hydrochar properties. Chemical Engineering Journal, 240: 574–578

van der Veen I, De Boer J (2012). Phosphorus flame retardants: properties, production, environmental occurrence, toxicity and analysis. Chemosphere, 88(10): 1119–1153

Vank J C, Henry-Riyad H, Csizmadia I G (2000). Successive protonation of phosphate (PO_4^{3-}), thiophosphate (PSO_3^{3-}), and selenophosphate ($PSeO_3^{3-}$). Journal of Molecular Structure THEOCHEM, 504(1–3): 267–286

Wan W, Zhang S, Huang H, Wu T (2016). Occurrence and distribution of organophosphorus esters in soils and wheat plants in a plastic waste treatment area in China. Environmental Pollution, 214: 349–353

Wang W, Deng S, Li D, Ren L, Shan D, Wang B, Huang J, Wang Y, Yu G (2018). Sorption behavior and mechanism of organophosphate flame retardants on activated carbons. Chemical Engineering Journal, 332: 286–292

Wei G, Li D, Zhuo M, Liao Y, Xie Z, Guo T, Li J, Zhang S, Liang Z (2015). Organophosphorus flame retardants and plasticizers: Sources, occurrence, toxicity and human exposure. Environmental Pollution, 196: 29–46

Xiang L, Wang X, Chen X, Mo C, Li Y, Li H, Cai Q, Zhou D, Wong M, Li Q X (2019). Sorption mechanism, kinetics and isotherms of di-n-butyl phthalate to different soil particle-size fractions. Journal of Agricultural and Food Chemistry, 67(17): 4734–4745

Xiao X, Chen B, Zhu L (2014). Transformation, morphology, and dissolution of silicon and carbon in rice straw-derived biochars under different pyrolytic temperatures. Environmental Science & Technology, 48(6): 3411–3419

Xiao X, Chen Z, Chen B (2016). H/C atomic ratio as a smart linkage between pyrolytic temperatures, aromatic clusters and sorption properties of biochars derived from diverse precursory materials. Scientific Reports, 6(1): 22644

Yan W, Yan L, Duan J, Jing C (2014). Sorption of organophosphate esters by carbon nanotubes. Journal of Hazardous Materials, 273: 53–

60

Yu Q, Zhang R, Deng S, Huang J, Yu G (2009). Sorption of perfluorooctane sulfonate and perfluorooctanoate on activated carbons and resin: Kinetic and isotherm study. Water Research, 43 (4): 1150–1158

Zhang G, Zhang Q, Sun K, Liu X, Zheng W, Zhao Y (2011). Sorption of simazine to corn straw biochars prepared at different pyrolytic temperatures. Environmental Pollution, 159(10): 2594–2601